

BIOCHEMISTRY

Fluoroalkylation promotes cytosolic peptide delivery

Guangyu Rong^{1*}, Changping Wang^{2*}, Lijie Chen¹, Yang Yan¹, Yiyun Cheng^{1,2†}

Cytosolic delivery of peptides remains a challenging task owing to their susceptibility to enzymatic degradation and the existence of multiple intracellular barriers. Here, we report a new strategy to address these issues by decoration of a fluororous tag on the terminal of cargo peptides. The fluororous-tagged peptides were assembled into nanostructures, efficiently internalized by cells via several endocytic pathways and released into the cytosol after endosomal escape. They were relatively stable against enzymatic degradation and showed much higher efficiency than nonfluorinated analogs and cell penetrant peptide-conjugated ones. The proposed strategy also efficiently delivered a proapoptotic peptide into specific sites in the cells and restored the function of cargo peptide after cytosolic delivery. The fluororous-tagged proapoptotic peptide efficiently inhibited tumor growth in vivo. This study provides an efficient fluorination strategy to promote the cytosolic delivery of peptides.

INTRODUCTION

Bioactive peptides are natural candidates to target the binding pockets of protein targets, especially for undruggable ones (1). Numerous peptides were identified as potent therapeutics in the treatment of bacterial and viral infections, cancers, and vascular diseases (2–4). These biomolecules showed unique advantages such as high selectivity, low toxicity, and excellent solubility in comparison with conventional chemical drugs that dominate the pharmaceutical industry (5, 6). However, peptides are prone to enzymatic degradation and thus have short half-life and poor bioavailability in vivo, which hindered the clinical translation of peptide drugs. In addition, current therapeutic peptides are limited toward extracellular targets such as cell surface receptors, ion channels, and secreted proteins due to the membrane impermeability of most peptides (1). The conjugation of cell penetrant peptides (CPPs) such as transactivator of transcription (TAT) or oligoarginines to cargo peptides is the most widely adopted strategy to facilitate cytosolic peptide delivery (7–9). However, CPP-decorated peptides are usually internalized by cells via endocytosis pathways and may suffer from entrapment within degradative or recycling vesicles during intracellular trafficking (10). These CPP-modified peptides are still susceptible to enzymatic degradation and need chemical modification such as cyclization to improve proteolytic stability and membrane permeability (11, 12).

Recently, polymers, rotaxanes, liposomes, and inorganic nanoparticles were used to deliver therapeutic peptides acting on intracellular protein targets (10, 13–17). For example, anionic polymers were complexed with positively charged peptides via electrostatic interactions (10). Lanthanide-doped inorganic nanoparticles were conjugated with cysteine-terminated peptides via covalent linkages (13). Alternatively, peptides themselves were fabricated into nanostructures via supramolecular assembly or genetic engineering for improved proteolytic stability and cytosolic internalization (18, 19). Despite these advantages, it remains a challenging task to develop a facile and robust strategy for cytosolic peptide delivery that can address the multiple extracellular and intracellular obstacles.

¹Shanghai Key Laboratory of Regulatory Biology, East China Normal University, Shanghai 200241, China. ²South China Advanced Institute for Soft Matter Science and Technology, School of Molecular Science and Engineering, South China University of Technology, Guangzhou 510640, China.

*These authors contributed equally to this work.

†Corresponding author. Email: yycheng@mail.ustc.edu.cn

Extensive research has shown that the incorporation of hydrophobic components such as alkyl chains, cholesterol, and hydrophobic amino acids to the backbone of peptides can facilitate its membrane permeability (20–23). The introduction of these hydrophobic ligands generates amphiphilic peptides that can self-assemble into various nanostructures (24, 25). This improves not only the endocytosis and endosomal escape of peptides but also their proteolytic stability (20). Our previous studies have found that fluorination notably improves the cellular uptake, endosomal escape, and serum stability of cationic polymers in gene and protein delivery (15, 26, 27). The fluorinated materials showed unique advantages in comparison with conventional lipid modified ones (15, 28). In addition, fluorinated materials have higher tendency to assemble into nanostructures than nonfluorinated ones due to extremely low surface energy (29, 30). Previously, several groups synthesized fluorinated peptides by incorporation of unnatural fluorinated amino acids, and these peptides showed excellent chemical and proteolytic stability, high association tendency in lipid bilayers, and unexpected folding behaviors (31–33). Combining these features together, we hypothesized that the decoration of a fluororous tag to peptides is responsive for improved proteolytic stability and cytosolic delivery efficacy. In this study, we added a cysteine to the terminus of cargo peptides and further conjugated the peptide with thiol-containing fluororous tags via the formation of degradable disulfide linkage. Cargo peptides with distinct physicochemical properties were assembled into nanostructures and internalized into cytosol (Fig. 1A). A proapoptotic peptide was also efficiently delivered inside cells, and the delivered cargo peptide successfully exerted its bioactivity by the proposed technique. The fluororous-tagged proapoptotic peptide exhibited potent anticancer activity in vivo.

RESULTS

Synthesis and cytosolic delivery of fluororous-tagged peptides

Six peptides (P1 to P6) with distinct charge property and hydrophobicity were chosen as cargo peptides (Fig. 1B). The peptides were conjugated with fluorescein isothiocyanate (FITC) at the N terminus. TAT and octaarginine (R8)-conjugated peptides were synthesized and used as positive controls. The cargo peptides were conjugated with fluororous tag **I** via the formation of a reduction-sensitive disulfide bond (table S1). The molecular weights of fluororous-tagged peptides were confirmed by electrospray ionization mass spectrometry (ESI-MS)

Copyright © 2020
The Authors, some
rights reserved;
exclusive licensee
American Association
for the Advancement
of Science. No claim to
original U.S. Government
Works. Distributed
under a Creative
Commons Attribution
NonCommercial
License 4.0 (CC BY-NC).

Downloaded from <http://advances.sciencemag.org/> on August 12, 2020

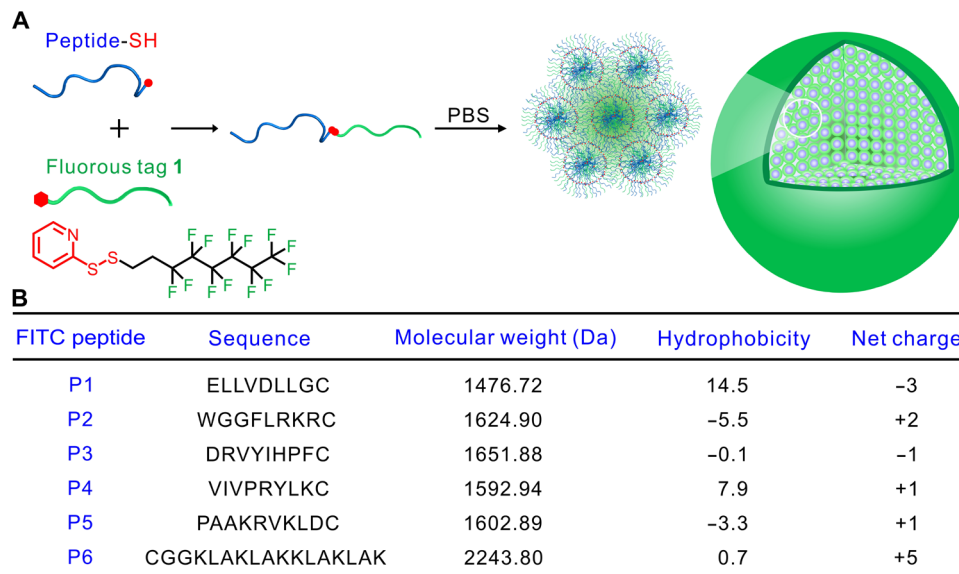


Fig. 1. Fluoroalkylation of peptides. (A) Fluoroalkylation leads to self-assembly of peptides into nanostructures. (B) Sequences, molecular weight, hydrophobicity, and net charge of cargo peptides in this study. The hydrophobicity of peptides was calculated according to Kyte-Doolittle hydrophobicity values (40).

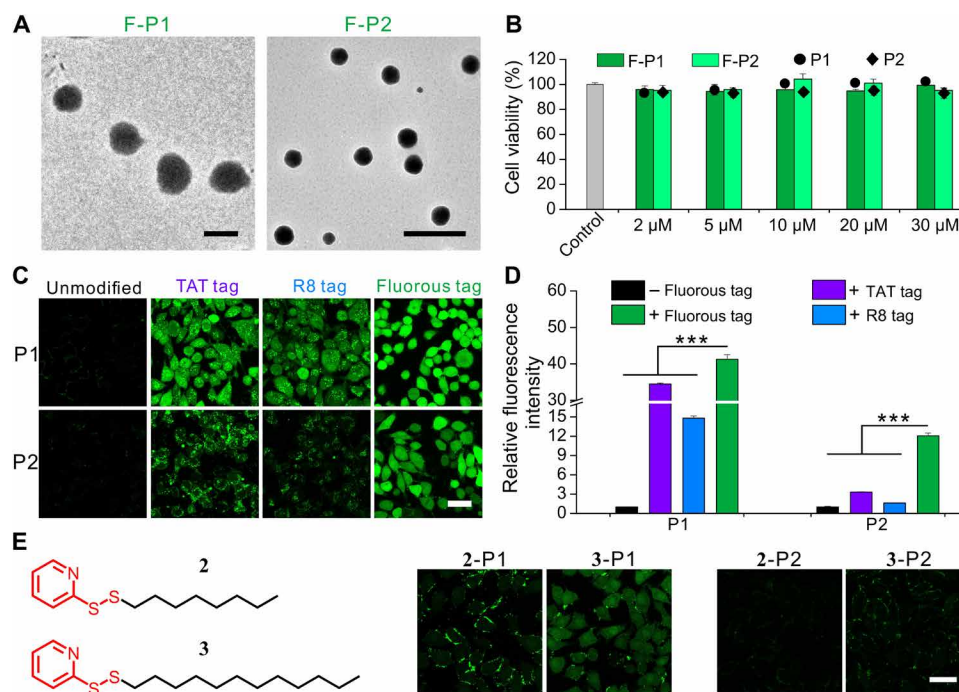


Fig. 2. Cytosolic delivery of fluoroalkylated peptides. (A) Transmission electron microscope (TEM) images of assembled F-P1 and F-P2. Scale bars, 500 nm. (B) The viability of HeLa cells treated with fluorous-tagged or unmodified peptides. Data are presented as means \pm SD ($n = 5$). (C) Confocal images of HeLa cells treated with peptides for 6 hours. Scale bar, 40 μ m. Unmodified, TAT-modified, and R8-modified peptides were tested as controls. Peptides (10 μ M) were tested for each sample. (D) Relative fluorescence intensity of cells treated with the peptides in (C). The fluorescence intensity of cells treated with unmodified peptides was defined as 1. Data are presented as means \pm SD ($n = 3$). *** $P < 0.001$ analyzed by one-factor analysis of variance (ANOVA). (E) Confocal images of HeLa cells treated with peptides modified with tag **2** or tag **3** for 6 hours (10 μ M peptide). Scale bar, 40 μ m.

(fig. S1). The tagged peptides were assembled into nanostructures in phosphate-buffered saline (PBS; pH 7.4) with particle dispersion index lower than 0.3 via a well-known fluorophilic effect (Fig. 2A and fig. S2A) (34). Elemental mapping result revealed that nitrogen (N), sulfur (S), and fluorine (F) elements were homogeneously dis-

tributed in the assembled nanoparticle (fig. S2B). Fluoroalkylation on peptides did not cause additional toxicity on the treated cells. All the fluorous-tagged peptides showed minimal toxicity on HeLa cells (Fig. 2B and fig. S2C). We then tested the cytosolic delivery of fluorinated nonapeptides P1 to P4 (F-P1, F-P2, F-P3, and F-P4,

respectively) on HeLa cells. The treated cells were observed by confocal microscope after 6-hour incubation, and the internalized peptides by cells were quantitatively measured by flow cytometry. Fluoroalkylation significantly promotes the cytosolic delivery of P1 to P4, and the delivery efficiencies are superior to TAT- or R8-tagged peptides at equal molar concentrations (Fig. 2, C and D, and fig. S2, D and E). Moreover, TAT- and R8-tagged peptides appear in punctate distributions in the treated cells. This is explained by the entrapment of peptides within endosomes and lysosomes after endocytosis (35). In contrast, the fluorescence from fluoroalkylated peptides is generally distributed throughout the cytosol, suggesting successful endosomal escape after cell uptake. After internalization, the release of cargo peptides from the assembled nanoparticles can be triggered by intracellular glutathione (GSH) due to the disulfide linkage between the fluorinated tag and cargo peptide. Take F-P1 for example, assembly of P1 into nanoparticles by fluoroalkylation results in decreased fluorescence intensity. However, the fluorescence of F-P1 is almost

recovered in the presence of 10 mM GSH (fig. S3), suggesting efficient release of cargo peptides. To reveal the fluorine effect of fluoroalkylated peptides during cytosolic delivery, we synthesized two types of nonfluorinated controls. The peptides P1 to P4 were tagged with alkyl tags 2 and 3 via the same chemistry. The alkyl tag 2 has the same number of carbon atoms with fluorinated tag 1. Considering that the contribution of a CF_2 group to hydrophobicity was about 1.5-fold that of a CH_2 group in alkyl chains (15), the hydrophobicity of alkyl tag 3 with 12 carbon atoms could be roughly equivalent to that of tag 1 with 8 carbon atoms. Alkylated peptides could also be assembled into nanoparticles in aqueous solutions due to their amphiphilic characteristics; however, the assembled nanostructures are not as uniform as those of fluorinated peptides (fig. S4). The superior behavior of fluoroalkylated peptides in assembly is attributed to the extremely low surface energy of fluoroalkyl chains compared to nonfluorinated controls. Peptides conjugated with the nonfluorinated tags show much weaker internalization by HeLa cells in comparison

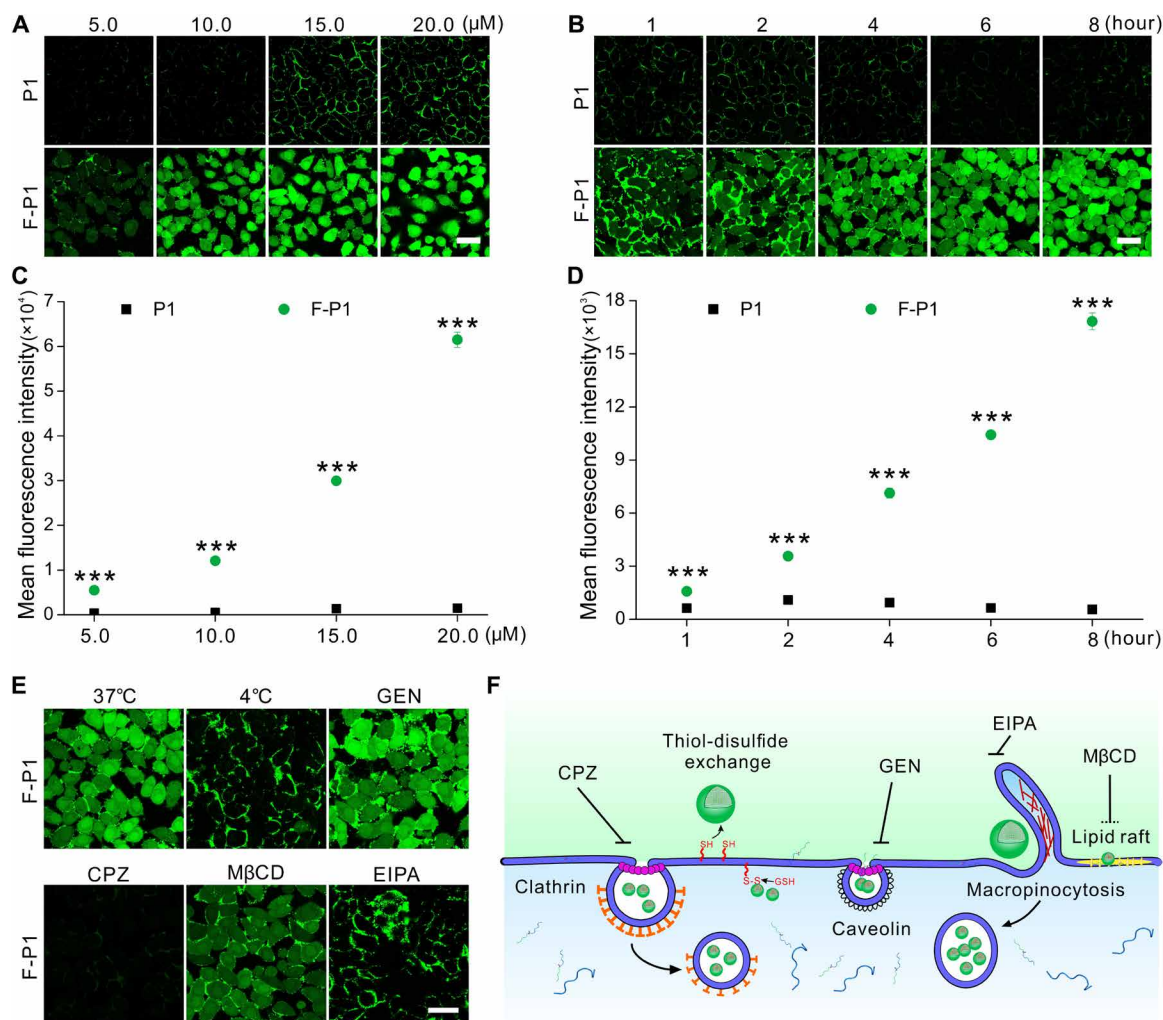


Fig. 3. Endocytosis pathways of fluorinated-tagged peptides. Confocal images of HeLa cells treated with different doses of P1 or F-P1 for 6 hours (A) or with 10 μM P1 or F-P1 for 1 to 8 hours (B). Scale bar, 40 μm. The fluorescence intensities of cells in (A) and (B) analyzed by flow cytometry are shown in (C) and (D), respectively. Data are presented as the means ± SD (n = 3). ***P < 0.001 analyzed by Student's t test. (E) Confocal images of HeLa cells treated with 10 μM F-P1 for 6 hours. The cells were pre-treated with different inhibitors before peptide incubation. Scale bar, 40 μm. (F) Proposed endocytosis pathways for F-P1.

with fluorinated ones (Fig. 2E and fig. S4D). The fluorescence of peptides modified with tag 2 or tag 3 is mainly observed on cell membranes. This can be explained by the fusion of lipid-functionalized peptides with phospholipids of cell membranes. On the other hand, the fluoroalkyl chains are both hydrophobic and lipophobic, and the mixing of fluorocarbons and hydrocarbons is highly nonideal (36). Therefore, the fluoroalkylated peptides are unlikely fused with the cell membranes during endocytosis. This result is in accordance with our previous finding that fluorinated polymers have higher membrane permeability than nonfluorinated ones (15). Besides P1 to P4, fluoroalkylation significantly improves the cytosolic delivery of a cationic and hydrophilic decapeptide P5 into HeLa cells. Fluorous-tagged P5 forms assembled nanostructures and shows much more efficient cell internalization than unmodified and TAT-conjugated P5 (fig. S2, F to H). We further investigated the effects of peptide dose and incubation time on the efficiency of fluorinated-tagged peptides. Take F-P1 for example, the fluorescence intensity of treated HeLa cells is in proportion to both peptide dose (Fig. 3, A and C) and incubation time (Fig. 3, B and D). F-P1 is mainly associated with cell membranes during the early period and efficiently internalized by the cells after 2 hours. In comparison, unmodified P1 shows poor cytosolic delivery at all the tested conditions. These results suggest the beneficial effect of fluoroalkylation on cytosolic peptide delivery. To reveal the endocytosis mechanism of F-P1 by HeLa cells, we pre-

treated the cells with various endocytosis inhibitors before the addition of F-P1. As shown in Fig. 3E, the internalization of F-P1 is notably inhibited at 4°C or in the presence of chlorpromazine (CPZ; inhibitor of clathrin-dependent endocytosis) and ethylisopropylamiloride (EIPA; inhibitor of macropinocytosis) while slightly influenced by methyl- β -cyclodextrin (M β CD; inhibitor of lipid raft) and genistein (GEN; inhibitor of caveolin-dependent endocytosis). It is reported that materials containing disulfide bonds can be internalized into cells via a thiol-disulfide exchange mechanism (37). To evaluate the possibility of this pathway during the internalization of F-P1, we pretreated HeLa cells with dithiothreitol (DTT; a reductant) or Ellman's reagent [5,5'-dithiobis-(2-nitrobenzoic acid) (DTNB); an oxidizer] before incubation with F-P1. As shown in fig. S5 (A and B), the internalization of F-P1 is increased to a certain degree by DTT but inhibited by DTNB. This is also evidenced by the phenomenon that part of the peptides is located on cell membranes at the early stages of incubation. These results together suggest that the endocytosis of fluoroalkylated peptides such as F-P1 is energy dependent and involved with multiple pathways including clathrin-dependent endocytosis, micropinocytosis, and the thiol-disulfide exchange mechanism (Fig. 3F). Besides F-P1, other fluoroalkylated peptides show similar endocytosis behaviors (figs. S5C and S6). The cells treated with F-P1 exhibit uniformly distributed fluorescence throughout the cytosol after 2-hour incubation, and the internalized peptides

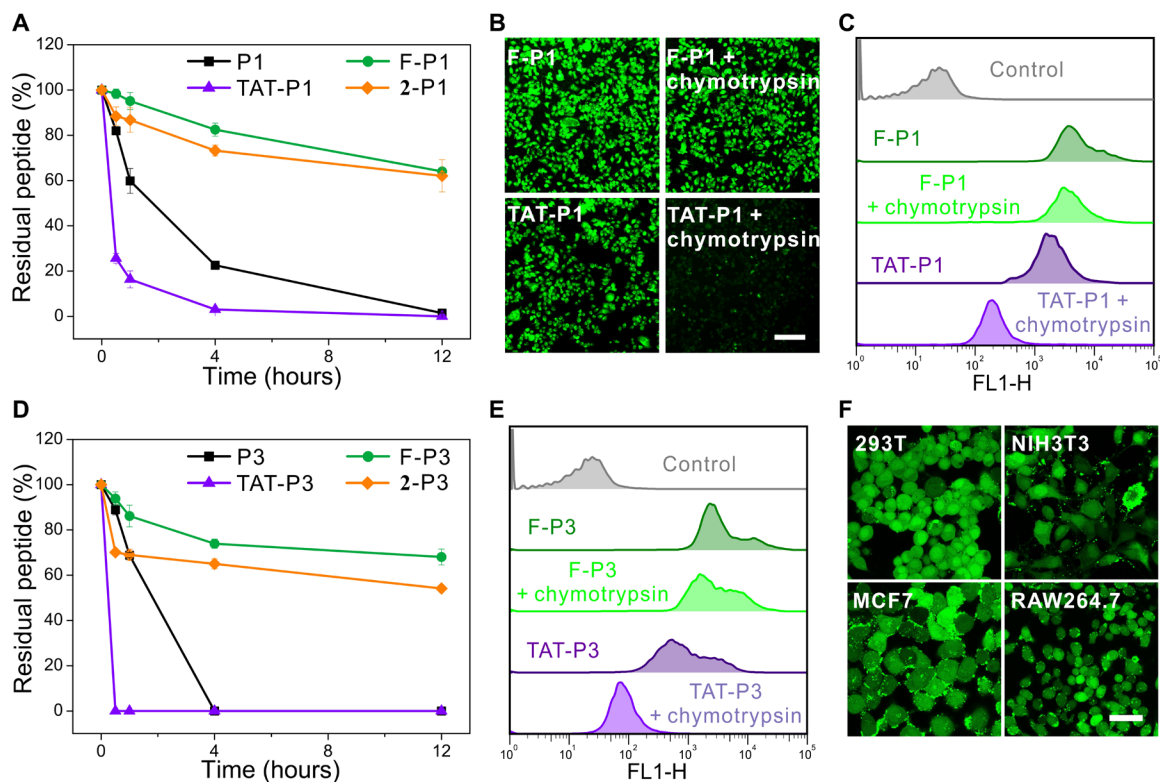


Fig. 4. Proteolytic stability of fluorinated-tagged peptides. (A) Degradation behavior of P1, TAT-P1, 2-P1, and F-P1 after incubation with chymotrypsin for 0 to 12 hours. Data are presented as the means \pm SD ($n = 3$). (B) Fluorescence images of HeLa cells treated with F-P1 or TAT-P1 for 6 hours. The peptides were added with chymotrypsin before cytosolic delivery to prove the proteolytic stability of F-P1. A representative result from three independent experiments. Scale bar, 200 μ m. (C) Flow cytometric analysis of peptide-incubated cells in (B). (D) Degradation behavior of P3, TAT-P3, 2-P3, and F-P3 after incubation with chymotrypsin for 0 to 12 hours. Data are presented as the means \pm SD ($n = 3$). (E) Flow cytometric analysis of HeLa cells treated with F-P3 or TAT-P3 for 6 hours. The cells were added without or with chymotrypsin during cytosolic delivery. (F) Cytosolic delivery of F-P1 into 293T, NIH3T3, MCF7, and RAW264.7 cells, respectively, for 6 hours. The concentration of F-P1 in each well is 10 μ M. Scale bar, 40 μ m.

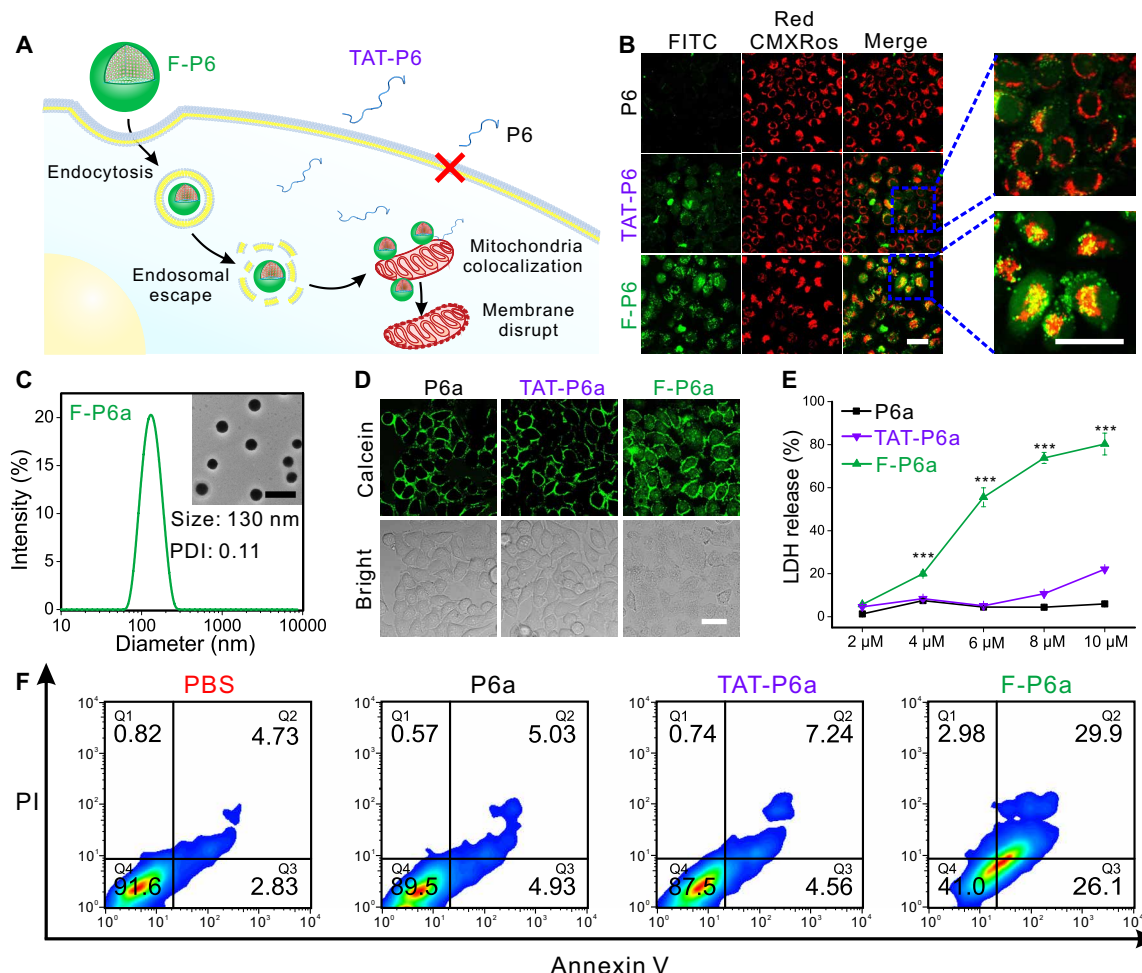


Fig. 5. Cytosolic delivery of fluoros-tagged KLA. (A) Cytosolic delivery of F-P6 into cancer cells induces cell apoptosis and death. (B) Confocal images of HeLa cells treated with 4 μ M FITC-labeled peptides P6, F-P6, or TAT-P6 for 6 hours. The mitochondria in cells were stained by MitoTracker Red CMXRos. Scale bar, 40 μ m. (C) TEM image and dynamic light scattering (DLS) of assembled F-P6a. Scale bar, 500 nm. (D) Confocal images of calcein-treated HeLa cells. The cells were incubated with 10 μ M P6a, F-P6a, or TAT-P6a for 6 hours before calcein treatment. Scale bar, 40 μ m. (E) LDH release from peptide-treated cells. Data are presented as means \pm SD ($n=3$). *** $P < 0.001$ analyzed by one-factor ANOVA. (F) Apoptosis of peptide-treated HeLa cells analyzed by an annexin V/propidium iodide (PI) staining assay. The cells were incubated with 10 μ M P6a, F-P6a, or TAT-P6a for 24 hours.

are not colocalized with acidic organelles (fig. S5D). The rapid endosomal escape of peptide nanoparticles via endocytosis might be attributed to the endosomal escape capability of fluoros-tagged peptides (15). The efficient endocytosis and endosomal escape of fluoros-tagged peptides are similar to our previous findings on fluorinated polymers (26, 27).

Proteolytic stability of fluoros-tagged peptides

The assembly of fluoros-tagged peptides into nanostructures may protect the peptides against protease degradation. In addition, the antifouling property of fluoroalkyl chains conjugated on peptides ensures high stability of assembled structures. We incubated the P1, F-P1, 2-P1, and TAT-P1 with chymotrypsin at 37°C for 0, 0.5, 1, 4, and 12 hours, respectively. The remaining F-P1 after treatment was quantitatively analyzed by reversed-phase high-performance liquid chromatography (HPLC). Unmodified P1, 2-P1, and TAT-P1 were tested as controls. As shown in Fig. 4A and fig. S7A, P1 and TAT-P1 are almost completely degraded in the presence of chymo-

trypsin at 12 hours; however, F-P1 and 2-P1 show better resistance to chymotrypsin. About 64% F-P1 and 62% 2-P1 remain in the solution after 12-hour incubation with chymotrypsin. Although 2-P1 also has potent proteolytic stability, it shows poor cytosolic delivery efficiency. We further compared the cytosolic delivery of F-P1 and TAT-P1 before and after chymotrypsin treatment. F-P1-treated cells maintain high fluorescence intensity in the presence of chymotrypsin (Fig. 4B), while TAT-P1-treated ones show weak fluorescence under the same condition, and the fluorescence intensity is decreased by an order of magnitude (Fig. 4C). The results clearly prove that F-P1 has better proteolytic stability than TAT-P1. Similar results are obtained on F-P2, F-P3, and F-P4 (Fig. 4, D and E, and figs. S7 and S8). The fluoroalkylated peptides such as F-P1 show robust efficiency in cytosolic delivery of peptides into various cell lines such as 293T, NIH3T3, MCF7, and RAW264.7 cells (Fig. 4F). The high proteolytic stability and robust delivery efficiency of fluoros-tagged peptides are essential for in vivo therapeutic applications.

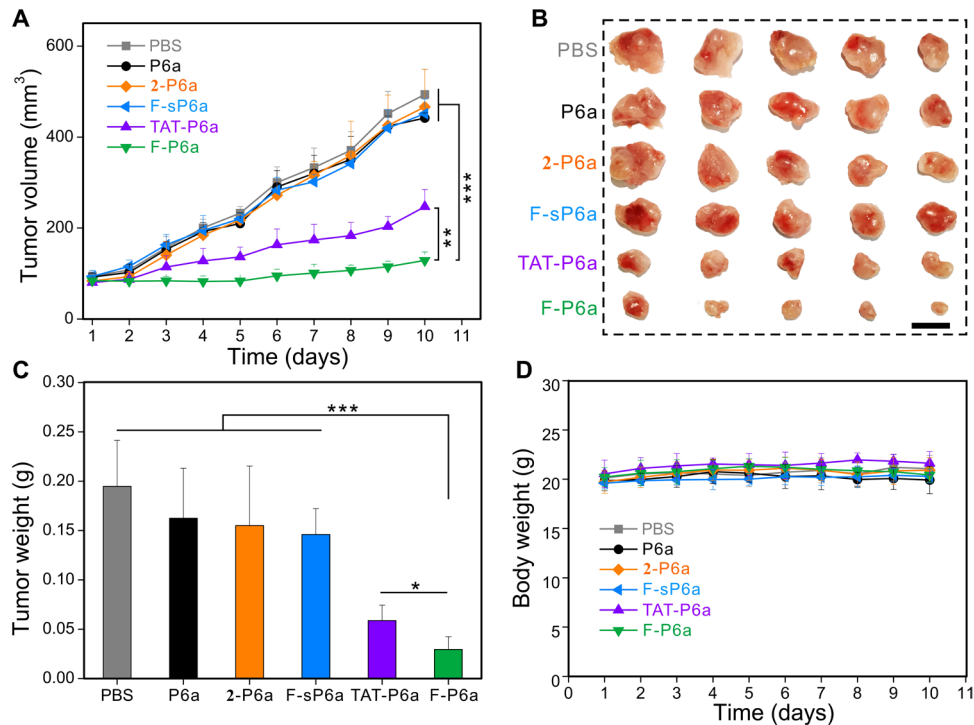


Fig. 6. Therapeutic effect of fluorour-tagged proapoptotic peptide KLA in vivo. (A) Tumor volume of mice treated with PBS, P6a, 2-P6a, F-sP6a, TAT-P6a, and F-P6a, respectively. Data are presented as means \pm SD ($n = 5$). $**P < 0.01$ and $***P < 0.001$ analyzed by one-factor ANOVA. (B) Image of excised tumors from the therapeutic groups. Scale bar, 1 cm. (C) Tumor weight in different groups. Data are presented as means \pm SD ($n = 5$). $*P < 0.05$ and $***P < 0.001$ analyzed by one-factor ANOVA. (D) Body weight of mice during the therapeutic period. Data are presented as means \pm SD ($n = 5$).

Fluoroalkylation promotes cytosolic delivery of bioactive peptides

We further investigated whether the bioactivity of fluorour-tagged peptides is maintained after cytosolic delivery. KLAKLAKLAKLAK (KLA) is a well-known proapoptotic peptide that induces cell apoptosis by disrupting mitochondrial membrane (38, 39). Although KLA is a cationic and amphipathic peptide, it has poor permeability across cell membranes. Therefore, KLA alone has minimal toxicity on the treated cells. To increase its anticancer activity, KLA was usually conjugated with CPPs such as TAT (39). We chose KLA as the bioactive cargo peptide. A cysteine group was added to the N terminus of KLA (P6) for fluoroalkylation (Fig. 5A). F-P6 assembles into nanoparticles around 120 nm in buffer (table S1) and is efficiently internalized into HeLa cells (Fig. 5B). The cytosolic delivery efficiency of F-P6 is much higher than those of unmodified P6, TAT-P6, 2-P6, and 3-P6 (Fig. 5B and fig. S4D). F-P6 exhibits similar endocytosis and cytosolic delivery behaviors with other fluorour-tagged peptides (figs. S5C and S6, I and J). Internalized F-P6 shows colocalization with mitochondria in HeLa cells stained by MitoTracker Red CMXRos. To distinguish the peptides with and without FITC labeling, they were termed P6 and P6a, respectively. F-P6a shows a similar assembly behavior with F-P6 (~130 nm; Fig. 5C). It causes notably enhancement of cell permeability to calcein, a membrane impermeable green fluorescent dye (Fig. 5D), and a significant increase in lactate dehydrogenase (LDH) release from the treated cells (Fig. 5E). The efficient cytosolic delivery of P6a into cancer cells by fluoroalkylation leads to much increased apoptosis (Fig. 5F) and cell death (fig. S9, A and B). On the contrary, the cells treated with unmodified P6a

and TAT-P6a showed intact membranes and much higher viability. Similar results are obtained on breast cancer MDA-MB-231 cells (fig. S9C). The cytotoxicities of nonfluorinated control peptides 2-P6a and 3-P6a are much lower than that of F-P6a. We also synthesized a scrambled P6a peptide (sP6a; CGLLAAKKKKKAALL) to confirm that the observed cytotoxicity is caused by the bioactive peptide. F-sP6a induces low cytotoxicity on MDA-MB-231 cells at equal concentrations (fig. S9C). These results suggest that fluoroalkylation not only promotes cytosolic delivery of cargo peptides but also keeps their bioactivity after intracellular delivery.

Fluoroalkylated KLA peptide for in vivo cancer therapy

We further investigated the anticancer activity of fluorour-tagged proapoptotic peptide P6 in nude mice bearing MDA-MB-231 tumors. The assembled F-P6a nanoparticles with size around 130 nm were proposed to accumulate in tumor via the enhanced permeability and retention effect of nanoparticles. As shown in Fig. 6A, the administration of F-P6a at a dose of 7.5 μ mol of peptide/kg of mice efficiently inhibits tumor growth, and the anticancer activity of F-P6a in vivo is superior to those of unmodified P6a, 2-P6a, F-sP6a, and TAT-P6a. The size and weight of excised tumors from the F-P6a group are also much lower than those of control groups (Fig. 6, B and C). F-P6a labeled with cyanine 5.5 (cy5.5) shows much prolonged blood circulation time compared to free peptides (fig. S9D). In addition, F-P6a_{Cy5.5} shows enhanced tumor accumulation in nude mice bearing MDA-MB-231 tumors (fig. S9E) than the free peptide. The treatment of mice with F-P6a did not cause obvious change in body weight (Fig. 6D) during the therapeutic period. In addition, we

examined the hematological parameters, liver function, and histological sections of normal nude mice treated with F-P6a and PBS, respectively. The results also confirm the low toxicity of F-P6a in vivo (fig. S9, F to I). Note that the current study is a proof of concept to provide an alternative technique to CPPs in cytosolic peptide delivery. There is a long way for the current nanoformulations to be used for therapeutic purpose.

DISCUSSION

In summary, we developed a fluoroalkylation strategy for efficient cytosolic peptide delivery. Several cargo peptides were efficiently delivered into cytosol by the fluoros tag. The internalized peptides can keep their bioactivity after intracellular delivery. A fluoroalkylated proapoptotic peptide exhibited potent anticancer activity in vitro and in vivo. The technique also showed much superior intracellular delivery efficiency and better proteolytic stability in comparison to CPPs such as TAT and oligoarginines. It provides a facile and promising alternative strategy to deliver membrane-impermeable peptides into cytosol.

MATERIALS AND METHODS

Materials

All the peptides (purity, >95%) were synthesized by GL Biochem (Shanghai, China). 1-Octanethiol, 1-dodecanethiol, 1*H*,1*H*,2*H*,2*H*-perfluoro-1-octanethiol, GEN, M β CD, CPZ, trypan blue, and Hoechst 33258 were obtained from Sigma-Aldrich (St. Louis, MO, USA). DTT and DTNB were purchased from Aladdin (Shanghai, China). 3-(4,5-Dimethylthiazol-2-yl)-2,5-diphenyltetrazolium bromide (MTT), acridine orange (AO), and ethidium bromide (EB) were purchased from Sangon Biotech (Shanghai, China). 2,2'-Dithiodipyridine, calcein, and chymotrypsin were obtained from Macklin (Shanghai, China). EIPA was provided by MedChemExpress (Monmouth Junction, NJ, USA).

Synthesis of fluoros tag 1

2,2'-Dithiodipyridine (521.5 mg, 2.4 mmol) was dissolved in 3.5 ml of methanol, and then 1*H*,1*H*,2*H*,2*H*-perfluoro-1-octanethiol (300 mg, 0.8 mmol) dissolved in 1.5 ml of methanol was added slowly. The reaction mixture was stirred for 12 hours at room temperature. After that, the solvent was removed by rotary evaporator. The product was then purified by column chromatography. The mobile phase was dichloromethane and methanol (30/1, v/v). The fluoros tag 1 was obtained as a pale-yellow colored oil (238.0 mg, yield 79.3%). The alkyl tag 2 and tag 3 were synthesized by the same procedure.

Synthesis of fluoros-tagged peptides

The fluoros-tagged peptides were synthesized via a facile chemistry. Take P1 for example, 5 mg of P1 (0.003 mmol) dissolved in 1 ml of methanol was added into a solution of fluoros tag 1 (4.4 mg, 0.0091 mmol) in dichloromethane. The reaction was accomplished at 4°C for 4 hours under argon atmosphere. The fluoros-tagged peptides were precipitated three times in diethyl ether. The products were then dried under vacuum and further purified by preparative thin-layer chromatography. Peptides modified with tag 2 or tag 3 were synthesized by a similar protocol. The purity of fluoros-tagged peptides was confirmed by HPLC (Agilent 1200, USA) and further characterized by ESI-MS (SHIMADZU LCMS-2020, Japan). Assembled

peptides with fluoros tags were prepared by the following procedure. The peptides were dissolved in dimethyl sulfoxide and slowly added into PBS by micropipette. The solvent of assembled nanoparticles was removed by ultrafiltration through a 3000-Da molecular weight cutoff membrane (Millipore, USA), and the nanoparticles were resuspended in PBS. The hydrodynamic sizes and zeta potential were determined with dynamic light scattering (DLS; Zetasizer Nano ZS90, Malvern, UK). Transmission electron microscope (TEM; HT7700, Hitachi, Japan) was used to observe the assembled nanostructures. The assembled nanostructure of F-P1 was also examined by elemental mapping (Talos F200 \times , FEI) to identify the distributions of nitrogen (N), sulfur (S), and fluorine (F) elements in the nanoparticle.

Cell culture

NIH3T3, MCF7, 293T, RAW264.7, and HeLa cells from American Type Culture Collection (ATCC) were cultured in Dulbecco's modified Eagle's medium (DMEM; Gibco) at 37°C under 5% (v/v) CO₂, and MDA-MB-231 cells (ATCC) were cultured in minimum essential medium (MEM; Gibco). The culture media were supplemented with 10% (v/v) fetal bovine serum (FBS; Gemini Bio), penicillin sulfate (100 U/ml; Gibco), and streptomycin (100 μ g/ml; Gibco).

Cytosolic delivery of peptides

The cells were seeded in 24-well plates overnight until 90% confluence. Fluoros-tagged peptides at various concentrations were diluted with 200 μ l of serum-free media and incubated with the cells for 0 to 6 hours. After incubation, the cells were washed three times with PBS and treated with trypan blue (0.2 mg/ml) for 1 min to quench the fluorescence of FITC-conjugated peptides adsorbed on cell surface. The cells were released from the plate using 0.25% (v/v) trypsin-EDTA and resuspended in PBS buffer before measurement by flow cytometry (BD FACSCalibur, USA) to quantitatively analyze the cytosolic delivery efficiency. Unmodified peptides and TAT- or R8-conjugated peptides were tested as controls. Three repeats were conducted for each sample. For confocal microscopy, the cells were seeded in glass bottom cell culture dishes, and a laser scanning confocal microscope (LSCM; Leica SP8, Germany) was used to observe the peptide-treated cells.

To investigate the endocytosis mechanism for fluoros-tagged peptides, endocytosis inhibitors including GEN (700 μ M), CPZ (20 μ M), M β CD (10 mM), or EIPA (100 μ M) were added to HeLa cells and treated for 1 hour at 37°C. After that, the medium was removed. Then, the cells were treated with peptides as described above. Cytosolic peptide delivery at 4°C was also conducted to prove the role of adenosine 5'-triphosphate during peptide delivery. Cells treated with fluoros-tagged peptides at 37°C but without any inhibitor pretreatment were tested as a control. The treated cells were lastly observed by LSCM as described above. To investigate the thiol-disulfide exchange mechanism during the internalization of fluoroalkylated peptides, 2 mM DTT or 2 mM DTNB was pre-incubated with HeLa cells for 20 min at 37°C. Subsequent processing was consistent with the protocols described above.

To monitor the localization of peptides (P6, F-P6, and TAT-P6) after cytosolic delivery, HeLa cells were incubated with peptides for 6 hours as described above. The mitochondria in cells were stained with MitoTracker Red CMXros (75 nM; Invitrogen) for 15 min at 37°C. After that, the cells were washed three times with PBS and observed by LSCM.

To measure the membrane leakage of cells after treatment with peptides, HeLa cells were treated with different peptides for 6 hours as described above. After that, the culture media were removed. Then, the cells were treated with calcein (10 μ M) for 10 min. The cells were then washed three times with PBS and observed by LSCM.

Cytotoxicity and apoptosis assay

The cytotoxicity of peptides and fluoros-tagged peptides on the treated cells was first determined by an MTT assay. In general, the cells were seeded in 96-well plates (10^4 cells per well) for 24 hours before MTT assay. Then, the cells were treated with different concentrations of peptides for 6 hours as described above. After that, the cells were replenished with fresh DMEM (10% FBS) and further incubated for 18 hours. The viability of treated cells was measured by a standard MTT assay. Cells without any treatment were set as 100% viability. All measurements were performed in quintuplicate.

For LDH assay, the cells were incubated with peptides (without FITC) of different concentrations for 24 hours at 37°C. After that, the supernatant in each well was transferred into a new plate and treated with lysis buffer for 1 hour at 37°C. Sixty microliters of working solution was then added into each well and incubated at room temperature for 30 min according to the manufacturer's protocol (Beyotime, Jiangsu). The absorbance of solution in each well at 490 nm was measured by a microplate reader. Cells without any treatment were tested as the negative control, while cells directly treated with lysis buffer for 1 hour were set as the positive control. The relative LDH release was calculated by $(\text{LDH\% sample} - \text{LDH\% negative}) / (\text{LDH\% positive} - \text{LDH\% negative}) \cdot 100\%$. Three repeats were conducted for each sample.

For AO/EB staining assay, HeLa cells were treated with the peptides (without FITC) for 24 hours as described above. After that, the culture media were removed, and the treated cells were washed with PBS. The cells were stained with AO (5 μ g/ml) and EB (5 μ g/ml) for 3 min. After that, the cells were washed with PBS and examined under a fluorescent microscope (Olympus, Japan).

For apoptosis assay, the cells were treated with peptides (without FITC) for 24 hours as described above. After that, the cells were resuspended in binding buffer and stained with FITC-annexin V/propidium iodide (PI) for 15 min according to the manufacturer's protocol (BD Biosciences, Shanghai). The stained cells in each well were analyzed by flow cytometry.

Proteolytic stability assay

To evaluate the proteolytic stability of peptides against chymotrypsin, the peptides were diluted to 1 mg/ml with PBS and added with chymotrypsin (1 mg/ml). The mixture was incubated at 37°C for different times. After that, the remaining peptides in the samples were analyzed by C18 reversed-phase HPLC. The mobile phase of HPLC was a mixture of acetonitrile and deionized water containing 0.1% trifluoroacetic acid. P1 and analog peptides were run under a linear gradient from 35% (v/v) acetonitrile at 0 min to 65% (v/v) acetonitrile at 25 min and then to 100% acetonitrile at 40 min. P2 and analog peptides were run under a linear gradient from 29% (v/v) acetonitrile at 0 min to 54% (v/v) acetonitrile at 25 min and then to 100% acetonitrile at 35 min. P3 and analog peptides were run under a linear gradient from 25% (v/v) acetonitrile at 0 min to 54% (v/v) acetonitrile at 25 min and then to 100% acetonitrile at 35 min. P4 and analog peptides were run under a linear gradient from 30% (v/v) acetonitrile at 0 min to 60% (v/v) acetonitrile at 25 min and then to 100% acetonitrile at 35 min. The flow rate was 1 ml/min. The samples were detected at 220 nm.

In vivo toxicity studies of fluoros-tagged KLA

All animal procedures were in agreement with the National Institutes of Health guidelines and approved by the ethics committee of the East China Normal University (ECNU). Specific pathogen-free female BALB/c nude mice of 4 weeks old with an average body weight of 20 g was purchased from SLAC Laboratory Animal Co. Ltd. (Shanghai, China).

For in vivo blood toxicity assay, normal nude mice were divided into two groups (five mice in each group). PBS (150 μ l) and F-P6a (150 nmol, 318 μ g) were intravenously injected into the mice. The injections were repeated at the third and fifth day. The blood was collected 5 days after the last treatment, the liver function was tested by a biochemistry analyzer (Chemray-800, Rayto, China), and hematological parameters were measured by a hematology analyzer (BC-2800Vet, Mindray, China). The livers in treated mice were collected, embedded in paraffin, sectioned, and stained with hematoxylin and eosin or terminal deoxynucleotidyl transferase-mediated deoxyuridine triphosphate nick end labeling (TUNEL). To determine the apoptosis level in liver tissues, a TUNEL assay was used. Briefly, the sections were incubated with TUNEL reaction mixture, proteinase K, and Hoechst 33258 according to the manufacturer's protocol (Roche, Mannheim, Germany). The stained tissue sections were observed by a fluorescent microscope (Olympus, Japan).

In vivo pharmacokinetics and biodistribution of fluoros-tagged KLA

For the pharmacokinetic study, P6 labeled with cy5.5 (P6_{Cy5.5}) (150 nmol, 348 μ g) or F-P6_{Cy5.5} (150 nmol, 405 μ g) was intravenously injected into BALB/c nude mice (~20 g). The blood was collected at the time points of 5 min, 0.5 hours, 1 hour, 2 hours, 4 hours, 6 hours, 12 hours, and 24 hours, respectively. The mice were euthanized after each time point, and three mice were repeated for each point. Then, the plasma was collected and diluted with PBS before measurement by a fluorescence spectroscopy (excitation, 625 nm; emission, 685 nm).

For the biodistribution study, P6_{Cy5.5} (150 nmol, 348 μ g) or F-P6_{Cy5.5} (150 nmol, 405 μ g) was intravenously injected into BALB/c nude mice (~20 g) bearing MDA-MB-231 tumors (90 mm³). The mice were euthanized at 24, 48, or 72 hours after injection. Then, the tumors were collected, and the fluorescence in the tumors was analyzed in vivo imaging system (Lumina II, Caliper Life Sciences).

In vivo therapeutic efficiency of fluoros-tagged KLA

Each BALB/c nude mice (~20 g) was injected subcutaneously with 10^6 MDA-MB-231 cells. The mice bearing tumor around 90 mm³ were classified into six groups (five mice in each group): PBS group, P6a group, 2-P6a group, F-sP6a group, TAT-P6a group, and F-P6a group. The mice were administrated with PBS (150 μ l), P6a (150 nmol, 261 μ g), 2-P6a group (150 nmol, 283 μ g), F-sP6a group (150 nmol, 318 μ g), TAT-P6a (150 nmol, 477 μ g), or F-P6a (150 nmol, 318 μ g), respectively, via tail vein injection. The injections were repeated at the first, third, and fifth day. The body weight and tumor size of the mice were recorded every day. The mice were euthanized at the 10th day.

SUPPLEMENTARY MATERIALS

Supplementary material for this article is available at <http://advances.sciencemag.org/cgi/content/full/6/33/eaaz1774/DC1>

[View/request a protocol for this paper from Bio-protocol.](#)

REFERENCES AND NOTES

- H. Acar, J. M. Ting, S. Srivastava, J. L. LaBelle, M. V. Tirrell, Molecular engineering solutions for therapeutic peptide delivery. *Chem. Soc. Rev.* **46**, 6553–6569 (2017).
- S. Pescina, C. Ostacolo, I. M. Gomez-Monterrey, M. Sala, A. Bertamino, F. Sonvico, C. Padula, P. Santi, A. Bianchera, S. Nicoli, Cell penetrating peptides in ocular drug delivery: State of the art. *J. Control. Release* **284**, 84–102 (2018).
- B. Gomes, M. T. Augusto, M. R. Felício, A. Hollmann, O. L. Franco, S. Gonçalves, N. C. Santos, Designing improved active peptides for therapeutic approaches against infectious diseases. *Biotechnol. Adv.* **36**, 415–429 (2018).
- M. Miragoli, P. Ceriotti, M. Iafiso, M. Vacchiano, N. Salvarani, A. Alogna, P. Carullo, G. B. Ramirez-Rodriguez, T. Patricio, L. D. Esposti, F. Rossi, F. Ravanetti, S. Pinelli, R. Alinovi, M. Erreni, S. Rossi, G. Condorelli, H. Post, A. Tampieri, D. Catalucci, Inhalation of peptide-loaded nanoparticles improves heart failure. *Sci. Transl. Med.* **10**, eaan6205 (2018).
- A. N. Zelikin, C. Ehrhardt, A. M. Healy, Materials and methods for delivery of biological drugs. *Nat. Chem.* **8**, 997–1007 (2016).
- I. W. Hamley, Small bioactive peptides for biomaterials design and therapeutics. *Chem. Rev.* **117**, 14015–14041 (2017).
- L. Peraro, J. A. Kritzer, Emerging methods and design principles for cell-penetrant peptides. *Angew. Chem. Int. Ed.* **57**, 11868–11881 (2018).
- M. Vazdar, J. Heyda, P. E. Mason, G. Tesei, C. Alloio, M. Lund, P. Jungwirth, Arginine “Magic”: Guanidinium like-charge ion pairing from aqueous salts to cell penetrating peptides. *Acc. Chem. Res.* **51**, 1455–1464 (2018).
- A. Walrant, S. Cardon, F. Burlina, S. Sagan, Membrane crossing and membranotropic activity of cell-penetrating peptides: Dangerous liaisons? *Acc. Chem. Res.* **50**, 2968–2975 (2017).
- B. C. Evans, K. M. Hocking, K. V. Kilchrist, E. S. Wise, C. M. Brophy, C. L. Duvall, Endosomolytic nano-polyplex platform technology for cytosolic peptide delivery to inhibit pathological vasoconstriction. *ACS Nano* **9**, 5893–5907 (2015).
- L. Peraro, Z. Zou, K. M. Makwana, A. E. Cummings, H. L. Ball, H. Yu, Y.-S. Lin, B. Levine, J. A. Kritzer, Diversity-oriented stapling yields intrinsically cell-penetrant inducers of autophagy. *J. Am. Chem. Soc.* **139**, 7792–7802 (2017).
- J. M. Wolfe, C. M. Fadzén, R. L. Holden, M. Yao, G. J. Hanson, B. L. Pentelute, Perfluoroaryl bicyclic cell-penetrating peptides for delivery of antisense oligonucleotides. *Angew. Chem. Int. Ed.* **57**, 4756–4759 (2018).
- J. Yan, W. He, S. Yan, F. Niu, T. Liu, B. Ma, Y. Shao, Y. Yan, G. Yang, W. Lu, Y. Du, B. Lei, P. X. Ma, Self-assembled peptide-lanthanide nanoclusters for safe tumor therapy: Overcoming and utilizing biological barriers to peptide drug delivery. *ACS Nano* **12**, 2017–2026 (2018).
- J. Lv, Q. Fan, H. Wang, Y. Cheng, Polymers for cytosolic protein delivery. *Biomaterials* **218**, 119358 (2019).
- Z. Zhang, W. Shen, J. Ling, Y. Yan, J. Hu, Y. Cheng, The fluorination effect of fluoroamphiphiles in cytosolic protein delivery. *Nat. Commun.* **9**, 1377 (2018).
- X. Wang, X. Bao, M. McFarland-Mancini, I. Isaacsohn, A. F. Drew, D. B. Smithrud, Investigation of the intracellular delivery of fluoresceinated peptides by a host-[2] rotaxane. *J. Am. Chem. Soc.* **129**, 7284–7293 (2007).
- B. P. Shah, N. Pasquale, G. De, T. Tan, J. Ma, K.-B. Lee, Core-shell nanoparticle-based peptide therapeutics and combined hyperthermia for enhanced cancer cell apoptosis. *ACS Nano* **8**, 9379–9387 (2014).
- X. Yu, X. Gou, P. Wu, L. Han, D. Tian, F. Du, Z. Chen, F. Liu, G. Deng, A. T. Chen, C. Ma, J. Liu, S. M. Hashmi, X. Guo, X. Wang, H. Zhao, X. Liu, X. Zhu, K. Sheth, Q. Chen, L. Fan, J. Zhou, Activatable protein nanoparticles for targeted delivery of therapeutic peptides. *Adv. Mater.* **30**, 1705383 (2018).
- T. Suma, J. Cui, M. Müller, S. Fu, J. Tran, K. F. Noi, Y. Ju, F. Caruso, Modulated fragmentation of proapoptotic peptide nanoparticles regulates cytotoxicity. *J. Am. Chem. Soc.* **139**, 4009–4018 (2017).
- S. Li, R. Zou, Y. Tu, J. Wu, M. P. Landry, Cholesterol-directed nanoparticle assemblies based on single amino acid peptide mutations activate cellular uptake and decrease tumor volume. *Chem. Sci.* **8**, 7552–7559 (2017).
- S. Pujals, J. Fernandez-Carreado, M. J. Kogan, J. Martinez, F. Cavellier, E. Giralt, Replacement of a proline with silapropine causes a 20-fold increase in the cellular uptake of a pro-rich peptide. *J. Am. Chem. Soc.* **128**, 8479–8483 (2006).
- T. Takeuchi, M. Kosuge, A. Tadokoro, Y. Sugiura, M. Nishi, M. Kawata, N. Sakai, S. Matile, S. Futaki, Direct and rapid cytosolic delivery using cell-penetrating peptides mediated by pyrenebutyrate. *ACS Chem. Biol.* **1**, 299–303 (2006).
- S. Katayama, H. Hirose, K. Takayama, I. Nakase, S. Futaki, Acylation of octarginine: Implication to the use of intracellular delivery vectors. *J. Control. Release* **149**, 29–35 (2011).
- K. Cheng, Y. Ding, Y. Zhao, S. Ye, X. Zhao, Y. Zhang, T. Ji, H. Wu, B. Wang, G. J. Anderson, L. Ren, G. Nie, Sequentially responsive therapeutic peptide assembling nanoparticles for dual-targeted cancer immunotherapy. *Nano Lett.* **18**, 3250–3258 (2018).
- G. Qi, Y. Gao, L. Wang, H. Wang, Self-assembled peptide-based nanomaterials for biomedical imaging and therapy. *Adv. Mater.* **30**, e1703444 (2018).
- M. Wang, H. Liu, L. Li, Y. Cheng, A fluorinated dendrimer achieves excellent gene transfection efficacy at extremely low nitrogen to phosphorus ratios. *Nat. Commun.* **5**, 3053 (2014).
- H. Wang, Y. Wang, Y. Wang, J. Hu, T. Li, H. Liu, Q. Zhang, Y. Cheng, Self-assembled fluorodendrimers combine the features of lipid and polymeric vectors in gene delivery. *Angew. Chem. Int. Ed.* **54**, 11647–11651 (2015).
- T. Zhang, Y. Huang, X. Ma, N. Gong, X. Liu, L. Liu, X. Ye, B. Hu, C. Li, J. Tian, A. Magrini, J. Zhang, W. Guo, J. Xing, M. Bottini, X. Liang, Fluorinated oligoethylenimine nanoassemblies for efficient siRNA-mediated gene silencing in serum-containing media by effective endosomal escape. *Nano Lett.* **18**, 6301–6311 (2018).
- C. Carrillo-Carrion, M. Atabakhshi-Kashi, M. Carril, K. Khajeh, W. J. Parak, Taking advantage of hydrophobic fluorine interactions for self-assembled quantum dots as a delivery platform for enzymes. *Angew. Chem. Int. Ed.* **57**, 5033–5036 (2018).
- Y. Cheng, Fluorinated polymers in gene delivery. *Acta Polym. Sin.* **8**, 1234–1245 (2017).
- M. He, K. Kumar, Antimicrobial activity and protease stability of peptides containing fluorinated amino acids. *J. Am. Chem. Soc.* **129**, 15615–15622 (2007).
- N. Naarmann, B. Bilgiçer, M. He, K. Kumar, C. Steinem, Fluorinated interfaces drive self-association of transmembrane α helices in lipid bilayers. *Angew. Chem. Int. Ed.* **45**, 2588–2591 (2006).
- U. I. M. Gerling, M. Salwiczek, C. D. Cadicamo, H. Erdbrink, C. Czekelius, S. L. Grage, P. Wadhvani, A. S. Ulrich, M. Behrends, G. Haufe, B. Koksche, Fluorinated amino acids in amyloid formation: A symphony of size, hydrophobicity and α -helix propensity. *Chem. Sci.* **5**, 819–830 (2014).
- Q. Xiao, S. E. Sherman, S. E. Wilner, X. Zhou, C. Dazen, T. Baumgart, E. H. Reed, D. A. Hammer, W. Shinoda, M. L. Klein, V. Percec, Janus dendrimersomes coassembled from fluorinated, hydrogenated, and hybrid Janus dendrimersomes as models for cell fusion and fission. *Proc. Natl. Acad. Sci. U.S.A.* **114**, E7045–E7053 (2017).
- C. L. Watkins, P. Brennan, C. Fegan, K. Takayama, I. Nakase, S. Futaki, A. T. Jones, Cellular uptake, distribution and cytotoxicity of the hydrophobic cell penetrating peptide sequence PFVYLL linked to the proapoptotic domain peptide PAD. *J. Control. Release* **140**, 237–244 (2009).
- M. P. Krafft, Fluorocarbons and fluorinated amphiphiles in drug delivery and biomedical research. *Adv. Drug Deliv. Rev.* **47**, 209–228 (2001).
- S. Aubry, F. Burlina, E. Dupont, D. Delaroche, A. Joliot, S. Lavielle, G. Chassaing, S. Sagan, Cell-surface thiols affect cell entry of disulfide-conjugated peptides. *FASEB J.* **23**, 2956–2967 (2009).
- H. Jung, S. Kim, R. Park, J. Park, I. Kim, B. Lee, Bladder tumor-targeted delivery of pro-apoptotic peptide for cancer therapy. *J. Control. Release* **235**, 259–267 (2016).
- H. Kim, S. Kim, H. Youn, J. Chung, D. Shin, K. Lee, The cell penetrating ability of the proapoptotic peptide, KLAKLAKLAKLAK fused to the N-terminal protein transduction domain of translationally controlled tumor protein, MLIYRDLISH. *Biomaterials* **32**, 5262–5268 (2011).
- J. Kyte, R. F. Doolittle, A simple method for displaying the hydropathic character of a protein. *J. Mol. Biol.* **157**, 105–132 (1982).

Acknowledgments

Funding: We appreciate the grants from the National Key R&D Program of China, Synthetic Biology Research (no. 2019YFA0904500), the National Natural Science Foundation of China (21725402), the Science and Technology Commission of Shanghai Municipality (17XD1401600), and the Guangdong Innovative and Entrepreneurial Research Team Program (2016ZT06C322). We are grateful for the support of the ECNU Multifunctional Platform for Innovation (011), the Flow Cytometry Core Facility and the Confocal Microscopy Facility at ECNU. **Author contributions:** G.R. conducted most experiments on material synthesis, characterization, and cytosolic peptide delivery, analyzed the data, and wrote the manuscript. C.W. conducted the animal studies. L.C. performed part of cytosolic peptide delivery experiments. Y.Y. conducted part of the therapeutic experiments. Y.C. designed and supervised the study and wrote the manuscript. All authors read and approved the manuscript. **Competing interests:** Y.C. and G.R. are inventors on a patent pending related to this work filed by ECNU with the State Intellectual Property Office of P.R. China (2020110330603.3, filed on 24 April 2020). **Data and materials availability:** All data needed to evaluate the conclusions in the paper are present in the paper and/or the Supplementary Materials. Additional data related to this paper may be requested from the corresponding authors. The materials used in this research can be provided by the corresponding author (Y.C.) pending scientific review and a completed material transfer agreement. Requests for the material should be submitted to the corresponding author (Y.C.).

Submitted 19 August 2019

Accepted 30 June 2020

Published 12 August 2020

10.1126/sciadv.aaz1774

Citation: G. Rong, C. Wang, L. Chen, Y. Yan, Y. Cheng, Fluoroalkylation promotes cytosolic peptide delivery. *Sci. Adv.* **6**, eaaz1774 (2020).

Fluoroalkylation promotes cytosolic peptide delivery

Guangyu Rong, Changping Wang, Lijie Chen, Yang Yan and Yiyun Cheng

Sci Adv 6 (33), eaaz1774.

DOI: 10.1126/sciadv.aaz1774

ARTICLE TOOLS

<http://advances.sciencemag.org/content/6/33/eaaz1774>

SUPPLEMENTARY MATERIALS

<http://advances.sciencemag.org/content/suppl/2020/08/11/6.33.eaaz1774.DC1>

REFERENCES

This article cites 40 articles, 2 of which you can access for free
<http://advances.sciencemag.org/content/6/33/eaaz1774#BIBL>

PERMISSIONS

<http://www.sciencemag.org/help/reprints-and-permissions>

Use of this article is subject to the [Terms of Service](#)

Science Advances (ISSN 2375-2548) is published by the American Association for the Advancement of Science, 1200 New York Avenue NW, Washington, DC 20005. The title *Science Advances* is a registered trademark of AAAS.

Copyright © 2020 The Authors, some rights reserved; exclusive licensee American Association for the Advancement of Science. No claim to original U.S. Government Works. Distributed under a Creative Commons Attribution NonCommercial License 4.0 (CC BY-NC).